Desalination and Water Treatment
www.deswater.com

doi: 10.5004/dwt.2017.21349

90 (2017) 7–15
September

Effect of aeration on $CaSO_4$ scaling in membrane distillation process

Jihyeok Choi, Yongjun Choi, Yongsun Jang, Yonghyun Shin, Sangho Lee*

School of Civil and Environmental Engineering, Kookmin University, Jeongneung-Dong, Seongbuk-Gu, Seoul, 136-702, Korea, Tel. +82-2-910-4529; Fax: +82-2-910-4939; emails: sanghlee@kookmin.ac.kr (S. Lee), cjh6563@gmail.com (J. Choi), choiyj1041@gmail.com (Y. Choi), cutymonkey5@naver.com (Y. Jang), shinyonghyun@naver.com (Y. Shin)

Received 4 February 2017; Accepted 20 August 2017

ABSTRACT

Although membrane distillation (MD) can treat high-salinity feedwater such as reverse osmosis (RO) brine and produced water, the control of fouling resulted from scale formation is mandatory in such applications. As one of the attempts to alleviate fouling and scaling, this study applied an in-line air injection into the feed inlet of the membrane module in MD systems. Experiments were carried out in a bench-scale direct contact membrane distillation systems using a saturated $CaSO_4$ solution as the model feedwater. It was revealed that the air injection was effective to retard flux decline due to $CaSO_4$ scale formation. As the air flow rate and feed flow velocity increased, the flux reduction volume concentration factor increased from 1.17 to a maximum of 1.27. The critical concentration factor (CCF) that is defined as the concentration factor of rapid flux decline increased by the aeration. Since the MD fouling due to scale formation was attributed to the bulk crystallization, it is likely that the aeration can control the deposition of crystal particles on the membrane surface. In addition, the feed flow velocity was found to be an important factor affecting the effectiveness of aeration for MD scale control.

Keywords: Membrane distillation; Fouling; Aeration; Scale formation; Crystallization

1. Introduction

Water shortage is becoming a serious problem all over the world, which results from an increase in water demand and a decrease in available water resources [1]. In this context, seawater desalination has drawn attention as an ongoing supply of freshwater from saline water sources. There are various desalination technologies including multi-stage flash distillation, multi-effect distillation, reverse osmosis (RO), and electrodialysis [2]. Among them, RO is a leading technology for seawater and brackish water desalination [3,4]. However, RO has a limited capability of treating high salinity feedwater. In general, RO cannot be applied to feedwater that exceeds total dissolved solids (TDS) of 45,000 mg/L [4]. Moreover, RO is an energy-intensive process and its energy consumption can account from 45% for up to 60% of the total cost of the RO desalination [5]. Accordingly, it is necessary to explore novel desalination technologies that have capability of treating high-salinity water with affordable energy consumption.

Membrane distillation (MD) is an emerging technology that can overcome the current limitations of RO [5–7]. It is a thermally driven separation process, in which only vapors transfer through a microporous hydrophobic membrane [7–13]. Since MD is less sensitive to feedwater TDS than RO [7,14], it is more suitable to treat feedwaters of high salinity. Moreover, MD is typically driven with low grade heat and is therefore suited for the utilization of waste heat from industrial processes or generators as well as heat from renewable energy sources [15,16].

However, one of challenges associated with the use of MD is membrane fouling due to scale formation [14,17–20]. If MD is applied to treat high salinity feedwaters, the potential for scale formation is high, leading to serious fouling due to depositions of crystals on the membrane surface [21]. In MD, fouling development by inorganic salts such as $CaSO_4$ and

* Corresponding author.

Presented at the 9th International Desalination Workshop: Sustainable Desalination (IDW 2016), 13–15 November 2016, Abu Dhabi, UAE.

$CaCO_3$ has been analyzed in detail, highlighting the influence of thermal operation and hydrodynamic condition on crystal size formation, wetting phenomena and scaling reversibility. Accordingly, it is essential to understand and control MD fouling due to scale formation [22–24].

The membrane fouling is an inevitable phenomenon due to the deposit of the contaminants on membrane surface and/or within membrane pores. In MD systems, there are two types of foulants, including particles/colloids and scale-forming ions. During the MD operation, particles may deposit on the membrane surface and block the membrane pores. In complete blocking, it is assumed that each particle reaching to the membrane surface blocks the membrane pores without superimposing with other particles and the pore area open to water flow is reduced by blocking membrane pores [25,26]. If the feed solution contains sparingly soluble salts such as $CaCO_3$, $CaSO_4$, and silica, fouling occurs due to scale formation. The mechanisms of MD scale formation may be divided into two main categories [27,28]. The first mechanism is surface crystallization [27]. Through the heterogeneous nucleation, the inorganic salts form thin crystal layer on the surface of the membrane. As a result, the effective surface area decreases due to surface crystallization. The other mechanism of bulk crystallization [27]. Through the homogeneous nucleation, the crystal particles are formed and suspended. They may also deposit on the surface of the membrane and create cake layer, leading to flux decline. These two mechanisms make the crystallization process difficult to predict and control [29].

Previous works on MD fouling and scale formation have focused on the analysis of fouling mechanisms, modification of membrane surface, and cleaning of fouled membranes [18–20]. Aeration has been also considered as a novel approach to control MD fouling [30–32]. Nevertheless, little information is available how aeration affects scale formation mechanisms in MD processes. Moreover, the effect of operating conditions on the aeration effect has not been widely investigated. Accordingly, this study focused on aeration effect on fouling control and $CaSO_4$ scale formation mechanisms in MD processes.

2. Materials and methods

2.1. DCMD with aeration

The Fig. 1(a) shows the schematic diagram of laboratory-scale direct contact membrane distillation (DCMD) system, which has apply aeration to MD membrane module. This system consists of a feed solution tank, a permeated water tank, two gear pumps, a heater, a water bath, an aeration generator and a plate-and-frame membrane module. The membrane cell was made of acrylic resin with depth, width, and length of 2, 20, and 60 mm, respectively. A hot feed and a cold distillate were supplied at constant flowrate using the two gear pumps. Air was directly injected into the feed solution and the amount of air was measured by an air flow meter. As shown in Fig. 1(b), the air bubbles flow in the channel of the flat-sheet MD module. The mass of permeated water collected and measured using an electronic balance connected to a personal computer. The experiments were duplicated to confirm the reproducibility. The run order was also randomized to minimize experimental errors.

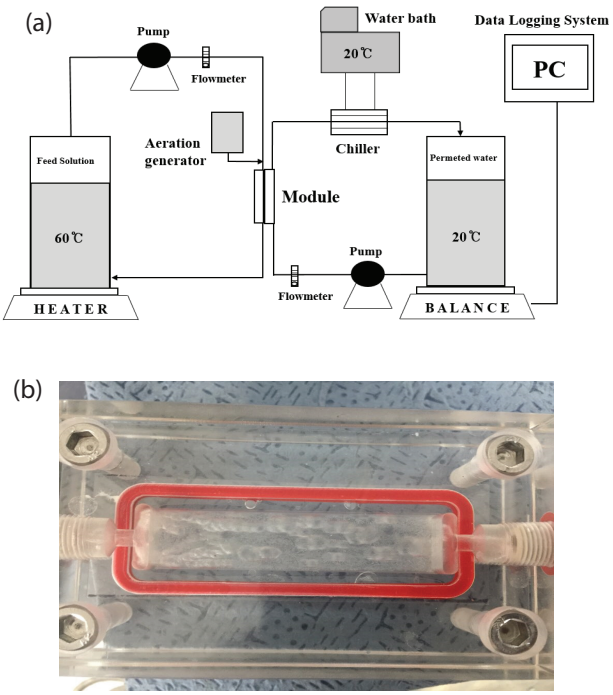

Fig. 1. (a) Schematic diagram of laboratory-scale DCMD system setup with in-line aeration; (b) flat sheet MD module with aeration.

2.2. Experimental conditions

A hydrophobic polyvinylidene fluoride (PVDF) flat sheet membrane, which has the nominal pore size of 0.22 μm was used. The effective membrane area was 12 cm^2. A feed solution containing $CaSO_4$ of 2,000 mg/L and 2 L volume was used as a feedwater for this experiment. The feed flow velocity was 8.33, 14.58, and 20.83 cm/s depending on the Reynolds number, respectively. The feed stream is recirculated over time to concentrate. The flow velocity of the distillate was 4.17, 8.33, 12.5 cm/s, respectively. The aeration was applied to MD module to control the fouling during the operation. The size of air bubbles were approximately 0.2–0.3 mm. The bubble size was measured by analyzing captured images by a digital camera (Samsung NX500, Korea), which had the resolution of 28 mega pixels. The temperature of feed solution and distillate were maintained at 60°C and 20°C, respectively, using a heater and a water bath. The operating conditions are summarized in Table 1.

2.3. Cartridge filter

Fig. 2 shows the cartridge filter (5 μm) used in experiment and the schematic diagram of laboratory-scale DCMD system with the cartridge filter. To distinguish surface crystallization and bulk crystallization, an on-line cartridge filter was applied to the MD system. The cartridge filter was installed after the feed into the membrane module to continuously remove the suspended crystal particles during the recirculation of the feed solution. Since the feed passed through the membrane at relatively high crossflow velocity, the location of the cartridge filter did not provide a

Table 1
Operating conditions for membrane distillation process

Operation type	Direct contact membrane distillation (DCMD)
Membrane type	PVDF flat sheet membrane
Effective membrane area	12 cm^2
Feed solution	$CaSO_4$ 2,000 ppm solution, 2 L
Feed flow velocity (cm/s)	8.33/14.58/20.83
Permeate flow velocity (cm/s)	4.17/8.33/12.5
Volume of air (mL/min)	100/200
Air bubbles size (mm)	0.2–0.3
Temperature (°C)	Feed side: 60 Permeate side: 20

noticeable difference. If fouling occurs with the use of the cartridge filter, it implies that the contribution of crystal particles in the bulk solution is negligible. In this case, it can be concluded the dominant scale formation mechanism surface crystallization. On the other hand, if fouling does not occur with the use of the cartridge filter, it suggests that the fouling is caused by the bulk crystals. Accordingly, bulk crystallization should be the domination fouling mechanism in such cases. In this study, a 5-μm cartridge filter was introduced to the recirculation line of the MD system to allow continuous removal of bulk crystals in the recirculating feed solution. The flux profiles without and with the cartridge filter were compared to determine which scale formation mechanism was dominant.

2.4. Field-emission electron microscope

A field-emission scanning electron microscope (FESEM; JSM-7610F) was used to identify morphology of fouling on membrane surface. In order to observe morphology of foulants, membranes were dried and coated by platinum. FESEM images could identify morphology of the scale shape and size depending on the flow rate and the amount of aeration.

3. Results and discussion

3.1. Fouling due to $CaSO_4$ scale formation in DCMD

Fig. 3 shows the changes in flux and turbidity during a DCMD experiment using the feedwater of $CaSO_4$ 2,000 mg/L solution. The feed and distillate flow velocity were 14.58 and 8.33 cm/s, respectively. The Reynolds number of the feed flow was 3,057, which corresponds to the transition zone. The Reynolds number is an important dimensionless quantity in fluid mechanics that used to help predict flow patterns in different fluid flow situations. The Reynolds number is given as:

$$\mathrm{Re} = \frac{\upsilon d \rho}{\eta} \quad (1)$$

where v is the mean velocity of the fluid (cm/s), d is the inside diameter if the pipe is circular (cm), ρ is the density of the fluid (g/cm^3) and η is the dynamic viscosity of the fluid (kg/m·s). Based on the calculated values, the experiment was conducted of feed flow velocity condition such as the laminar flow, the transition zone and the turbulent flow.

The feed and distillate temperatures were 60°C and 20°C, respectively. The results were shown as a function of volume concentration factor (VCF), which is the ratio of remaining feed volume (or retentate) to the initial feed volume.

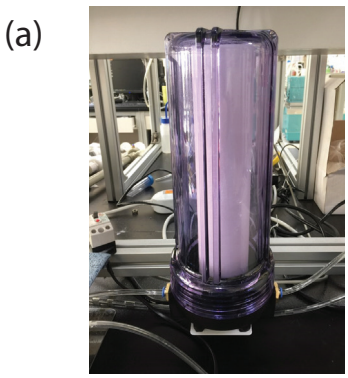

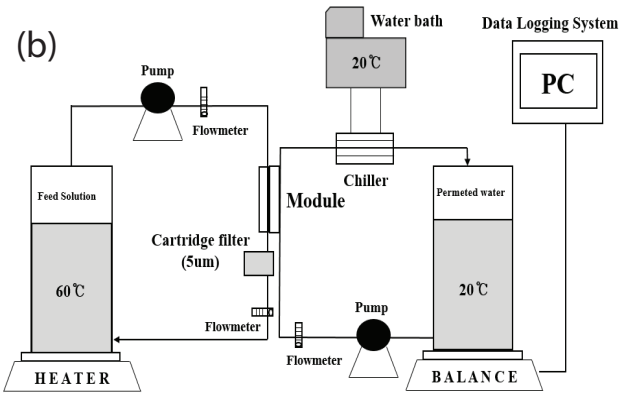

Fig. 2. (a) Cartridge filter of 5 μm; (b) schematic diagram of laboratory-scale DCMD system with cartridge filter.

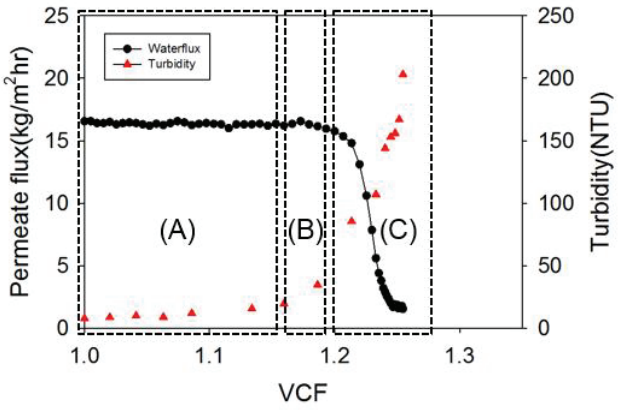

Fig. 3. Changes in flux and feedwater turbidity with VCF during DCMD operation without cartridge filter. (A) Induction period, (B) initial fouling period, (C) rapid fouling period.

As illustrated in Fig. 3, there were three stages of DCMD operation. The first stage was the induction period ranging from VCF of 1.0 to VCF of 1.17. During this stage, there was no flux decline, suggesting that no fouling occurred. Although the feed solution was saturated with $CaSO_4$, it takes time to initiate the crystal formation. In fact, the turbidity of the feedwater slightly increased after VCF of 1.12, indicating that $CaSO_4$ crystal formation occurred in the bulk phase under this condition. The second stage was the initial fouling period. Between VCF of 1.17 and 1.21, MD flux was gradually reduced and the turbidity of the feedwater quickly increased. It is likely that fouling occurred due to the formation of crystals in the bulk phase.

The final stage is the rapid fouling period. After VCF of 1.21, the flux rapidly decreased with an increase in the feedwater turbidity. In this period, not only bulk crystallization but also surface crystallization occurred, leading to MD fouling. Since the surface crystallization began from the VCF of 1.17, it was presumed that it continued above this VCF. The driving force of the surface crystallization is the higher concentration of inorganic ions near the membrane surface due to the concentration polarization. Accordingly, if bulk crystallization occurs, surface crystallization also occurs. Similar behaviors were also reported in the literature [27]. Nevertheless, it is not possible to quantitatively estimate the contributions of the two crystallization mechanisms from the results in Fig. 3 because both bulk and surface crystals existed at the same time.

3.2. Application of cartridge filter in MD to determine dominant fouling mechanism

To determine the domination crystallization mechanism in the DCMD system, the 5-μm cartridge filter was introduced to continuously remove bulk crystals. Under this condition, MD fouling due to bulk crystallization was suppressed. As shown in Fig. 4, the flux maintained constant from the beginning and no flux decline was observed up to VCF of 1.5.

Considering the fact that the flux decline occurred after VCF of 1.17 without the cartridge filter (Fig. 3), it is evident that MD fouling did not occur in the presence of the cartridge filter up to VCF of 1.5. The test was ended at VCF of 1.5 because it took more than 50 h to reach the VCF and thus it does not seem to be meaningful to have a longer operation time in a batch system. These results imply that the MD fouling by bulk crystallization is much more important than that by surface crystallization. In other words, the surface crystallization had negligible effect on fouling and thus bulk crystallization is the dominant mechanism of the flux decline due to crystal formation.

To visually confirm the results in Fig. 4, the membrane surfaces were examined using FESEM after the MD tests. Figs. 5(a) and (b) show the MD membranes without the cartridge filter (Fig. 3) and with the cartridge filter (Fig. 4), respectively. It is evident from the SEM images that the amount of foulants was much smaller when the cartridge filter was used. Moreover, the crystal particles on the membrane surface was loosely deposited and do not seem to affect the MD flux. The difference in the amount of crystal deposition is attributed to the suppression of bulk crystallization. Accordingly, it can be also concluded that the bulk crystallization is the dominant fouling mechanisms in this DCMD system.

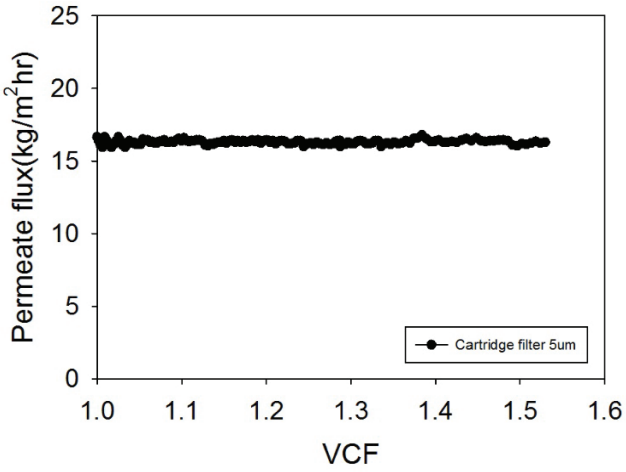

Fig. 4. Changes in flux with VCF with application of cartridge filter in MD.

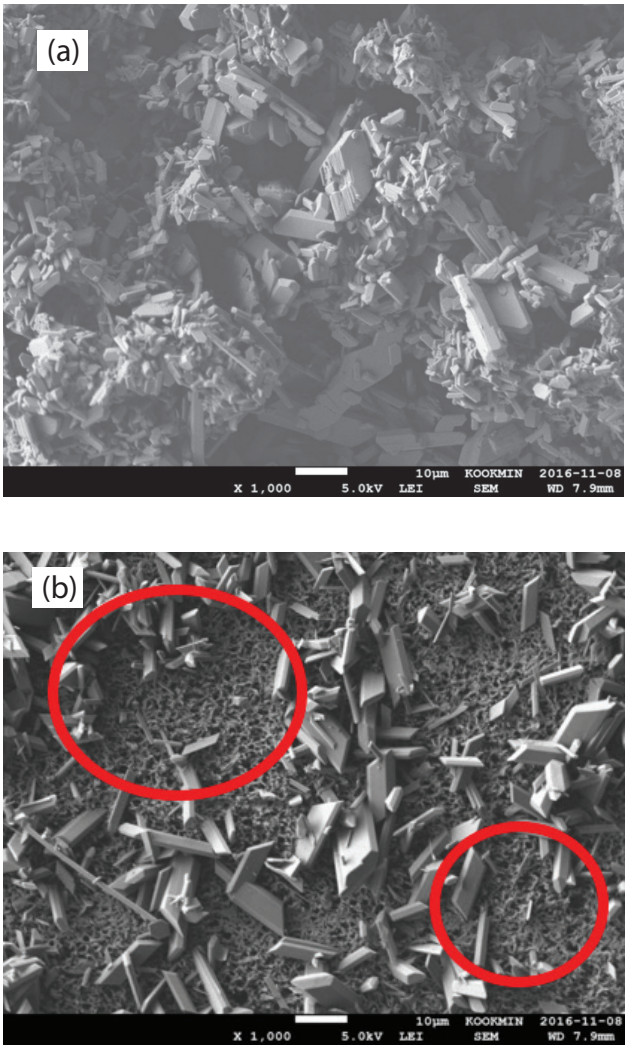

Fig. 5. FESEM images, (a) MD membrane without the use of cartridge filter, (b) MD membrane with the use of cartridge filter, red circles indicate the membrane surface without the deposition of crystal particles.

3.3. Effect of feed flow velocity on MD fouling due to scale formation

The feed flow velocity is one of the important factors affecting MD flux decline due to scale formation. If the feed flow velocity is high, the deposition of the bulk crystals is interfered, leading to decreased fouling. On the other hand, the flow velocity of distillate is not important because it cannot directly affect the formation of fouling layer on the membrane surface. To quantitatively examine the effect of feed flow velocity, MD experiments were carried out by varying the feed flow velocity to 8.33, 14.58, and 20.83 cm/s as depicted in Fig. 6. The corresponding Reynolds numbers were 1,747 (laminar flow), 3,057 (transition flow), and 4,367 (turbulent flow), respectively. As expected, flux decline in MD was reduced with an increase in the feed flow velocity. Moreover, the critical concentration factor (CCF) that is defined as the concentration factor of rapid flux decline increased by the aeration increased with the feed flow velocity, indicating that fouling due to scale formation is mitigated [27]. Nevertheless, above VCF of 1.24, a rapid flux decline occurred even at the highest feed flow velocity. Accordingly, it is necessary to apply additional techniques to further control MD fouling due to scale formation.

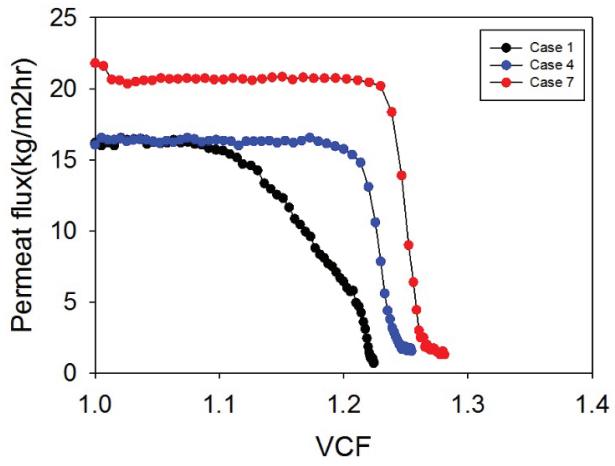

Fig. 6. Effect of feed flow velocity on flux decline due to scale formation (Case 1: 8.33 cm/s, Case 2: 14.58 cm/s, Case 3: 20.83 cm/s).

3.4. Effect of aeration on MD fouling

To mitigate MD fouling, the air flow was applied to the feed side of the MD system. A series of experiments were carried out to examine the effect of aeration on MD scale formation under three feed flow velocities. Two air flow rates including 0.1 and 0.2 L/min were considered. The experiments of cases are summarized in Table 2 and the results are shown in Fig. 7.

As expected, the air bubbles in the membrane channel retarded the deposition of bulk crystal particles on the membrane surface, leading to a decrease in flux decline. When the feed flow velocity was 8.33 cm/s (Fig. 7(a)), the initial flux was averagely 16.3 kg/m^2 h. The CCF value without aeration was 1.08 while those with the air flow rate of 100 and 200 mL/min were 1.14 and 1.18, respectively. With the feed flow velocity of 14.58 cm/s (Fig. 7(b)), the initial flux was averagely 16.9 kg/m^2 h, which was similar to that of 8.33 cm/s. However, the CCF value without aeration was 1.17 while those with the air flow rate of 100 mL/min and 200 mL/min were 1.20 and 1.23, respectively. When the feed velocity was 20.83 cm/s, the initial flux was the highest, which was 21.9 kg/m^2 h. In this case, the CCF value without aeration was found to be 1.23 while those with the air flow rate of 100 mL/min and 200 mL/min were 1.24 and 1.27, respectively. These results suggest that the aeration was effective to mitigate MD scale formation regardless of the feed flow velocities. Nevertheless, the effect of the aeration was the most important at the high feed flow velocity, as indicated in Fig. 7(c). The reduction in MD scale formation by the aeration was attributed to the scouring effect of air bubbles flowing in the MD module.

Fig. 8 compares the changes in feedwater turbidity during the MD experiments shown in Fig. 7. At the feed flow velocity of 8.33 cm/s, the aeration did not affect the feedwater turbidity. However, with the feed velocity of 14.58 and 20.83 cm/s, the feedwater turbidity slightly decreased with the application of the aeration. For example, the feedwater turbidity at VCF of 1.25 without aeration was 200 NTU at the feed flow velocity of 14.58 cm/s while that with the aeration of 200 mL/min was only 25 NTU. In addition, the feedwater turbidity at VCF of 1.25 without aeration was 170 NTU at the feed flow velocity of 20.83 cm/s while that with the aeration of 200 mL/min was 20 NTU. These results suggest that the amount of bulk crystals decreased

Table 2
Summary of experimental conditions

Case	Reynold's number	Feed flow velocity (cm/s)	Permeate flow velocity (cm/s)	Aeration (mL/min)	dT (°C)
1	1,747 (Laminar flow)	8.33	4.17	0	40
2		8.33	4.17	100	
3		8.33	4.17	200	
4	3,057 (Transition	14.58	8.33	0	
5	zone)	14.58	8.33	100	
6		14.58	8.33	200	
7	4,367 (Turbulent flow)	20.83	12.5	0	
8		20.83	12.5	100	
9		20.83	12.5	200	

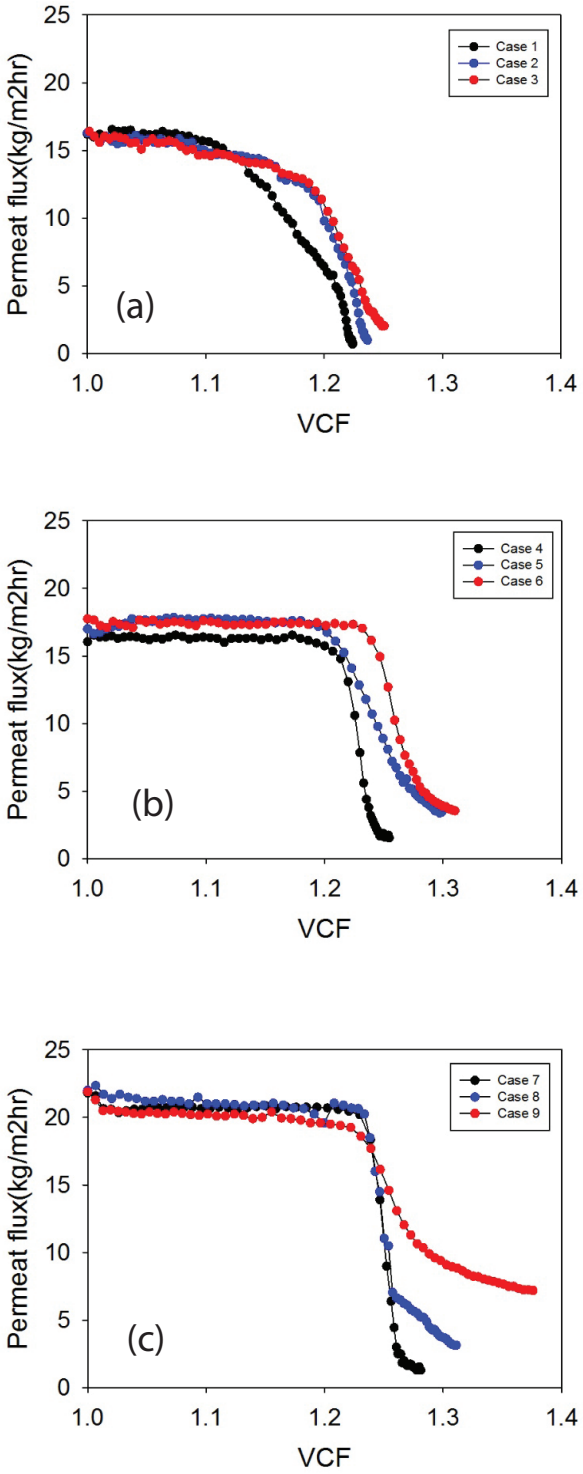

Fig. 7. The flux decline graphs based on VCF, (a) Cases 1–3 the flux decline when Laminar flow, (b) Cases 4–6 the flux decline graph when transition zone, (c) Cases 7–9 the flux decline graph when turbulent flow. The condition for each case is given in Table 2.

by applying the aeration, which may be another reason why the aeration is effective to control MD fouling due to bulk crystal formation.

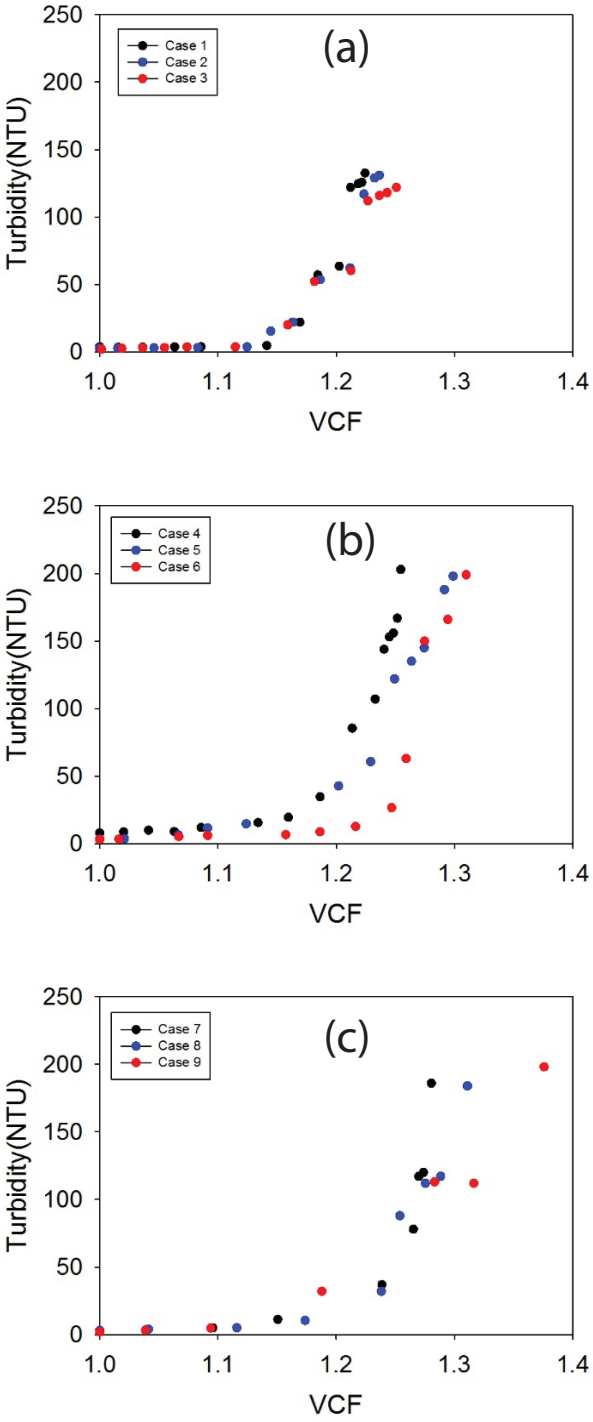

Fig. 8. The turbidity graphs based on VCF, (a) Cases 1–3 the turbidity at VCF point, (b) Cases 4–6 the turbidity at VCF point, (c) Cases 7–9 the turbidity at VCF point. The condition for each case is given in Table 2.

3.5. FESEM analysis of MD membrane surfaces

After the MD experiments, the surface of the membranes was examined using the FESEM. Fig. 9 shows the imagesof membrane surface covered by crystal scales. The size and

morphology of the crystals were analyzed under different feed flow velocities and aeration conditions. At the feed flow velocity of 8.33 cm/s without the aeration, the size of the crystals on the membrane surface was the largest. The crystal size decreases with an increase in the feed flow velocity as well as the air flow rate. The smallest crystals were found at the feed flow velocity of 20.83 cm/s with aeration of 200 mL/min.

There are two reasons for these results. As pointed out in the previous section, the formation of bulk crystals was retarded by the application of the aeration. This implies that the rate of crystal formation decreased, thereby affecting the size of the bulk crystals. The evidence for this was confirmed by measuring the turbidity. At higher air flow rates, turbidity increased later, another reason of the shear effect by the feed flow and aeration. Since the wall shear rate near the membrane increases with feed flow velocity and aeration intensity, relatively large crystal particles cannot be deposited due to the back transport to the bulk solution phase. In fact, it is likely that these two effects simultaneously occurred in this MD system (Fig. 9).

3.6. Comparison of CCF

In Fig. 10, the CCF values were summarized as a function of the feed flow velocity and aeration intensity. As increasing the feed flow velocity and the aeration intensity, the CCF increased. The lowest CCF was 1.08 at the feed flow velocity of 8.33 cm/s and no aeration. The highest CCF was 1.27 at the feed flow velocity of 20.83 cm/s and the aeration of 200 mL/min. It is interesting to note that the CCF can be increased by applying aeration instead of increasing the feed

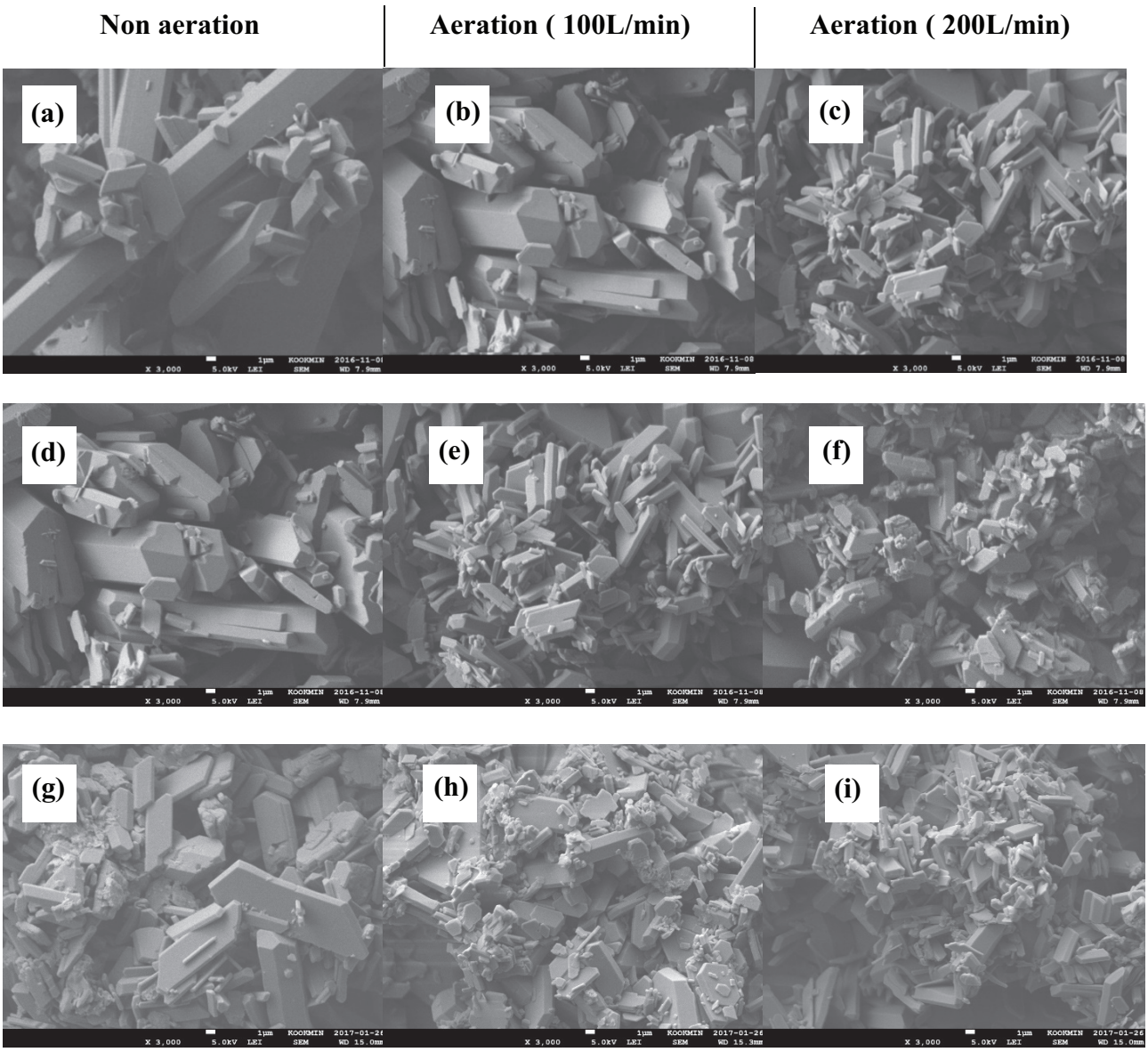

Fig. 9. FESEM (magnified to 3,000) photograph after MD experiments with aeration, (a)–(c) Laminar flow, (d)–(f) Transition zone, (g)–(i) Turbulent flow.

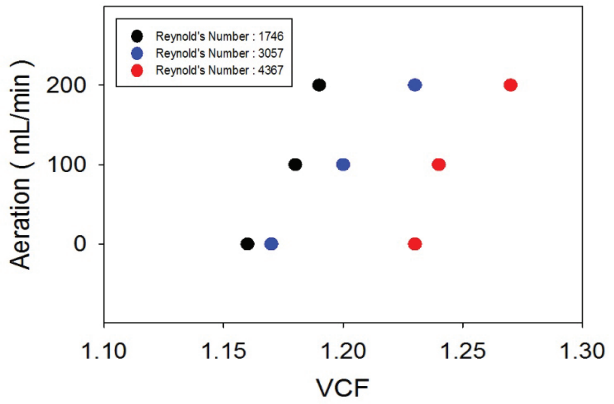

Fig. 10. Effect of aeration on CCF for MD scale formation under different flow velocities.

flow velocity. For example, the CCF at the feed flow velocity of 8.33 cm/s with the aeration of 100 mL/min is higher than that at the feed flow velocity of 14.58 cm/s without aeration. Moreover, the CCF at the feed flow velocity of 14.58 cm/s with the aeration of 200 mL/min is higher than that at the feed flow velocity of 20.83 cm/s without aeration. In fact, the aeration is less expensive than the increase in the feed flow velocity because the ratio of the air flow to the feed flow ranges from 0.2 to 0.5. Accordingly, it is likely that the aeration is an energy-efficient method to control MD scale formation.

4. Conclusion

In this study, the application of in-line aeration was attempted to control membrane fouling due to scale formation in DCMD systems and the following conclusions were withdrawn:

- It was found that there were three stages of MD membrane fouling due to scale formation during the treatment of $CaSO_4$ saturated solution, including the induction period, the initial moderate fouling period, and the rapid fouling period. The MD experiments using the on-line cartridge filter revealed that the MD fouling due to $CaSO_4$ scale formation was mainly caused by the bulk crystallization.
- An increase in the feed flow velocity resulted in a reduction in MD flux decline due to scale formation. This is attributed to the fact that the deposition of the bulk crystals is interfered with increased feed flow velocity.
- The application of aeration into the feed flow led to a decrease in the MD scale formation. The CCF, which is defined as the concentration factor of rapid flux decline, increased by the aeration. After the MD experiments, the surface of the membranes were examined using the FESEM. The crystal size decrease with an increase in the feed flow velocity as well as the air flow rate.
- As increasing the feed flow velocity and the aeration intensity, the CCF increased. It is possible that the CCF increases by applying aeration instead of increasing the feed flow velocity. Since the aeration is less expensive than the increase in the feed flow velocity, it is desired to apply aeration to mitigate MD scale formation.
- Although the addition of external aeration to the MD system was found to be effective, a techno-economic analysis will be required by considering the increase in flux and total cost (including capital and operational costs) to confirm if this is economically feasible.

Acknowledgment

This research was supported by a grant (code 16IFIP-B065893-04) from Industrial Facilities & Infrastructure Research Program funded by Ministry of Land, Infrastructure and Transport of Korean government.

References

[1] K.L. Lam, P.A. Lant, K.R. O'Brien, S.J. Kenway, Comparison of water-energy trajectories of two major regions experiencing water shortage, J. Environ. Manage., 181 (2016) 403–412.
[2] K.C. Kang, P. Linga, K.-n. Park, S.-J. Choi, J.D. Lee, Seawater desalination by gas hydrate process and removal characteristics of dissolved ions (Na^+, K^+, Mg^{2+}, Ca^{2+}, B^{3+}, Cl^-, SO_4^{2-}), Desalination, 353 (2014) 84–90.
[3] D. Zhou, L. Zhu, Y. Fu, M. Zhu, L. Xue, Development of lower cost seawater desalination processes using nanofiltration technologies—a review, Desalination, 376 (2015) 109–116.
[4] I. Wenten, Reverse osmosis applications: prospect and challenges, Desalination, 391 (2016) 112–125.
[5] A. Alkhudhiri, N. Darwish, N. Hilal, Membrane distillation: a comprehensive review, Desalination, 287 (2012) 2–18.
[6] F.A. Banat, F.A.A. Al-Rub, R. Jumah, M. Al-Shannag, Modeling of desalination using tubular direct contact membrane distillation modules, Separ. Sci. Technol., 34 (1999) 2191–2206.
[7] G. Naidu, S. Jeong, Y. Choi, S. Vigneswaran, Membrane distillation for wastewater reverse osmosis concentrate treatment with water reuse potential, J. Membr. Sci., 524 (2017) 565–575.
[8] L.D. Tijing, Y.C. Woo, J.-S. Choi, S. Lee, S.-H. Kim, H.K. Shon, Fouling and its control in membrane distillation—a review, J. Membr. Sci., 475 (2015) 215–244.
[9] F.A. Al-Rub, F.A. Banat, M. Shannag, Theoretical assessment of dilute acetone removal from aqueous streams by membrane distillation, Separ. Sci. Technol., 34 (1999) 2817–2836.
[10] F.A. Banat, F. Abu Al-Rub, R. Jumah, M. Shannag, On the effect of inert gases in breaking the formic acid–water azeotrope by gas-gap membrane distillation, Chem. Eng. J., 73 (1999) 37–42.
[11] F.A. Banat, F.A. Al-Rub, R. Jumah, M. Shannag, Theoretical investigation of membrane distillation role in breaking the formic acid-water azeotropic point: comparison between Fickian and Stefan-Maxwell-based models, Int. Commun. Heat Mass Transfer, 26 (1999) 879–888.
[12] F.A. Banat, F. Abu Al-Rub, R. Jumah, M. Al-Shannag, Application of Stefan–Maxwell approach to azeotropic separation by membrane distillation, Chem. Eng. J., 73 (1999) 71–75.
[13] F.A. Banat, F.A. Al-Rub, M. Shannag, Simultaneous removal of acetone and ethanol from aqueous solutions by membrane distillation: prediction using the Fick's and the exact and approximate Stefan-Maxwell relations, Heat Mass Transfer, 35 (1999) 423–431.
[14] B. Ashoor, S. Mansour, A. Giwa, V. Dufour, S. Hasan, Principles and applications of direct contact membrane distillation (DCMD): a comprehensive review, Desalination, 398 (2016) 222–246.
[15] D. Winter, J. Koschikowski, F. Gross, D. Maucher, D. Düver, M. Jositz, T. Mann, A. Hagedorn, Comparative analysis of full-scale membrane distillation contactors-methods and modules, J. Membr. Sci., 524 (2017) 758–771.
[16] J. Ge, Y. Peng, Z. Li, P. Chen, S. Wang, Membrane fouling and wetting in a DCMD process for RO brine concentration, Desalination, 344 (2014) 97–107.

[17] N. Ghaffour, J. Bundschuh, H. Mahmoudi, M.F. Goosen, Renewable energy-driven desalination technologies: a comprehensive review on challenges and potential applications of integrated systems, Desalination, 356 (2015) 94–114.
[18] Q.-M. Nguyen, S. Lee, Fouling analysis and control in a DCMD process for SWRO brine, Desalination, 367 (2015) 21–27.
[19] N. Hamzah, C. Leo, Fouling prevention in the membrane distillation of phenolic-rich solution using superhydrophobic PVDF membrane incorporated with TiO_2 nanoparticles, Separ. Purif. Technol., 167 (2016) 79–87.
[20] S. Meng, Y. Ye, J. Mansouri, V. Chen, Fouling and crystallisation behaviour of superhydrophobic nano-composite PVDF membranes in direct contact membrane distillation, J. Membr. Sci., 463 (2014) 102–112.
[21] C.A. Quist-Jensen, F. Macedonio, D. Horbez, E. Drioli, Reclamation of sodium sulfate from industrial wastewater by using membrane distillation and membrane crystallization, Desalination, 401 (2017) 112–119.
[22] L.D. Nghiem, T. Cath, A scaling mitigation approach during direct contact membrane distillation, Separ. Purif. Technol., 80 (2011) 315–322.
[23] F. He, J. Gilron, H. Lee, L. Song, K.K. Sirkar, Potential for scaling by sparingly soluble salts in crossflow DCMD, J. Membr. Sci., 311 (2008) 68–80.
[24] G. Naidu, S. Jeong, S. Vigneswaran, Interaction of humic substances on fouling in membrane distillation for seawater desalination, Chem. Eng. J., 262 (2015) 946–957.
[25] M. Aslam, A. Charfi, G. Lesage, M. Heran, J. Kim, Membrane bioreactors for wastewater treatment: a review of mechanical cleaning by scouring agents to control membrane fouling, Chem. Eng. J., 307 (2017) 897–913.
[26] M. Aslam, P.-H. Lee, J. Kim, Analysis of membrane fouling with porous membrane filters by microbial suspensions for autotrophic nitrogen transformations, Separ. Purif. Technol., 146 (2015) 284–293.
[27] Y. Shin, J. Sohn, Mechanisms for scale formation in simultaneous membrane distillation crystallization: effect of flow rate, J. Ind. Eng. Chem., 35 (2016) 318–324.
[28] D.M. Warsinger, J. Swaminathan, E. Guillen-Burrieza, H.A. Arafat, J.H. Lienhard V, Scaling and fouling in membrane distillation for desalination applications: a review, Desalination, 356 (2015) 294–313.
[29] D.M. Warsinger, E.W. Tow, J. Swaminathan, J.H. Lienhard V, Theoretical framework for predicting inorganic fouling in membrane distillation and experimental validation with calcium sulfate, J. Membr. Sci., 528 (2017) 381–390.
[30] G. Chen, X. Yang, R. Wang, A.G. Fane, Performance enhancement and scaling control with gas bubbling in direct contact membrane distillation, Desalination, 308 (2013) 47–55.
[31] S. Meng, Y.-C. Hsu, Y. Ye, V. Chen, Submerged membrane distillation for inland desalination applications, Desalination, 361 (2015) 72–80.
[32] D.M. Warsinger, A. Servi, S. Van Belleghem, J. Gonzalez, J. Swaminathan, J. Kharraz, H.W. Chung, H.A. Arafat, K.K. Gleason, J.H. Lienhard V, Combining air recharging and membrane superhydrophobicity for fouling prevention in membrane distillation, J. Membr. Sci., 505 (2016) 241–252.